IOP Publishing Smart Materials and Structures
Smart Mater. Struct. **25** (2016) 065019 (14pp) doi:10.1088/0964-1726/25/6/065019

Two-dimensional resonance frequency tuning approach for vibration-based energy harvesting

Lin Dong, M G Prasad and Frank T Fisher

Department of Mechanical Engineering, Stevens Institute of Technology, Hoboken, NJ 07030, USA

E-mail: ldong@stevens.edu and ffisher@stevens.edu

Received 18 September 2015, revised 25 January 2016
Accepted for publication 16 March 2016
Published 13 May 2016

Abstract

Vibration-based energy harvesting seeks to convert ambient vibrations to electrical energy and is of interest for, among other applications, powering the individual nodes of wireless sensor networks. Generally it is desired to match the resonant frequencies of the device to the ambient vibration source to optimize the energy harvested. This paper presents a two-dimensionally (2D) tunable vibration-based energy harvesting device via the application of magnetic forces in two-dimensional space. These forces are accounted for in the model separately, with the transverse force contributing to the transverse stiffness of the system while the axial force contributes to a change in axial stiffness of the beam. Simulation results from a COMSOL magnetostatic 3D model agree well with the analytical model and are confirmed with a separate experimental study. Furthermore, analysis of the three possible magnetization orientations between the fixed and tuning magnets shows that the transverse parallel magnetization orientation is the most effective with regards to the proposed 2D tuning approach. In all cases the transverse stiffness term is in general significantly larger than the axial stiffness contribution, suggesting that from a tuning perspective it may be possible to use these stiffness contributions for coarse and fine frequency tuning, respectively. This 2D resonant frequency tuning approach extends earlier 1D approaches and may be particularly useful in applications where space constraints impact the available design space of the energy harvester.

Keywords: frequency tuning, energy harvesting, vibration

(Some figures may appear in colour only in the online journal)

1. Introduction

Energy harvesting is a rapidly growing field with tremendous envisioned impact when integrated with ubiquitous wireless microsensors; for example, where embedded wireless microsensors are used to provide continuous monitoring of machine and structural health [1–3]. Although it is desirable to replace wired sensors with wireless sensors, many wireless sensor nodes are battery-powered [4], which means that there could be hundreds or thousands of batteries that need to be replaced during the anticipated lifetimes of the embedded nodes in a large sensor network. To replace each battery is tedious and expensive, especially when the device is in a remote location. In addition, a sensor node generally consists a microcontroller, transceiver, external memory, power source and one or more sensors. With advances in MEMS technology, the sizes of the microcontroller, transceiver, and external memory are decreasing rapidly, although battery technology is not allowing for the size of the batteries to decrease at the same rate [4]. Hence batteries may restrict further decreases in the total size and weight of the wireless sensor nodes. It is thus desirable to provide the wireless sensors with alternative types of power sources focusing on the characteristics of small volume, long lifetime, and greater reliability. One manner to provide this alternative power source is the field of vibration energy harvesting, where one seeks to convert ambient vibrations present in an environment to small but useful levels of electrical energy which could sufficiently

 © 2016 IOP Publishing Ltd Printed in the UK

power the nodes of these wireless sensor networks. A summary of vibration based energy harvesting for wireless, self-powered microsystems is well discussed in a review [5].

However, a clear need for a resonance-based vibration energy harvesting approach is a means to tune the resonant frequency of the device to match the source environmental frequency in order to achieve maximum power output. A comprehensive review of strategies for tuning the frequency range of vibration based energy harvesting has been described in the literature [6]. Several reported energy harvesters are designed to enable the resonant frequencies to match the possible ambient vibration frequencies based on applying external forces in either the horizontal or vertical direction with respect to the cantilever beam. For example, Yao *et al* [7] proposed a tunable energy harvester where the frequency can be tuned via the application of an electrostatic force. Their experimental results showed that the resonant frequency may increase or decrease with the applied tuning voltage depending on where the tuning electrode is placed with respect to the excitation electrode and the resonating rod, and a linear tuning range of 60 kHz (for an untuned resonant frequency of 960 kHz) was found with respect to the transverse tuning force with a maximum required DC tuning voltage of 35 V. Leland *et al* [8] designed a tunable-resonance vibration energy scavenger by using a transverse compressive preload on a piezoelectric bimorph with a tuning rage from 200 to 250 Hz. Challa *et al* [9] presented a resonance frequency tunable energy harvesting approach which applied a magnetic force perpendicular to the cantilever beam and was able to achieve tuning to ±20% of the unturned frequency based on the mode (attractive, repulsive) of the magnetic force. In addition, Zhu's group [10] designed a horizontal tunable electromagnetic vibration-based micro-generator, where the horizontal magnetic force induces variable axial loads on the cantilever beam. The resonant frequency was tuned from 67.6 to 98 Hz with the distance between the fixed and tuned magnets adjusted by an actuator.

In previous work the tuning operations are performed in one (transverse or axial) direction. In this paper, the tuning methodology is further developed and extended to allow the magnetic forces to be controlled by positioning of the magnets in a two-dimensional (2D) space. This 2D tuning principle is based on the effective stiffness theory. By applying magnetic forces in 2D space, the resonant frequency is related to two additional stiffnesses added to the system, which are referred to as the transverse stiffness and axial stiffness. While the expression for the transverse magnetic stiffness has been described previously [9], for purposes of this approach it is necessary to develop an analogous expression for the axial stiffness as a function of magnet separation as described below. Both theoretical calculations by MATLAB and simulation results from a COMSOL magnetostatics 3D model for the magnetic tuning forces of transverse force and axial force are discussed. Furthermore, analysis of the three possible magnetization orientations (transverse parallel, axial parallel, and cross magnetization direction) between the fixed and tuning magnets shows that the transverse parallel magnetization orientation is the most effective with regards to the proposed 2D tuning approach. Lastly, an experimental case study is described which verifies the results of the 2D tuning model.

2. 2D tuning mechanism

In the following sections, an overview of the 2D magnetic resonant frequency tuning approach is first presented, followed by a discussion of the considerations of the corresponding transverse and axial tuning components, respectively. Theoretical calculations of the magnetic transverse and axial forces between two magnets as a function of their relative positions in 2D space are discussed, with simulations based on COMSOL magnetostatics 3D model conducted to verify those magnetic forces obtained analytically. The effects of these applied magnetic forces on the overall device stiffness are then presented. Lastly, applicable constraints with respect to the practical implementation of the design of this 2D tuning method are briefly highlighted.

2.1. Tuning model

A schematic of the 2D resonant frequency magnetic tuning approach is shown in figure 1. The energy harvester is based on a two layer (PZT and Silicon layers) cantilever beam configuration; a fixed magnet is attached to the tip mass, and the tuning magnet moves in 2D space. Because the magnets are separated in 2D space, the respective locations of the magnets result in applied external transverse and axial forces on the cantilever beam. The principle of this 2D magnetic tuning approach is developed based on effective stiffness theory, where the transverse magnetic force results in a transverse magnetic stiffness and the axial magnetic force contributes to the axial stiffness of the system. The resonant frequency tuning operation is implemented by changing the position of the tuning magnet.

Three different magnetization orientations (transverse parallel, axial parallel and cross magnetization direction) as shown in figures 1(a)–(c) are analyzed in this 2D tuning approach. While in earlier 1D magnetic tuning work, the direction of the magnetic orientation for optimal tuning was clear (transverse magnetic orientation for the case of transverse magnetic tuning [9] and axial magnetic orientation for the case of axial magnetic tuning [10], respectively), for the 2D case the selection of which magnetic orientation to use is not clear. The distance between the two vertical axes of the magnets is d_a, while d_t is the distance between the bottom of the tuning magnet and top of the fixed magnet. The parameters of the cantilever beam and magnets in this research are given in table 1.

2.2. Tuning mechanism

Based on the general model of a second-order spring-mass-damper system for the conversion of mechanical vibration to electrical power [11], the effective stiffness is schematically shown in figure 2. Here the system is represented with three

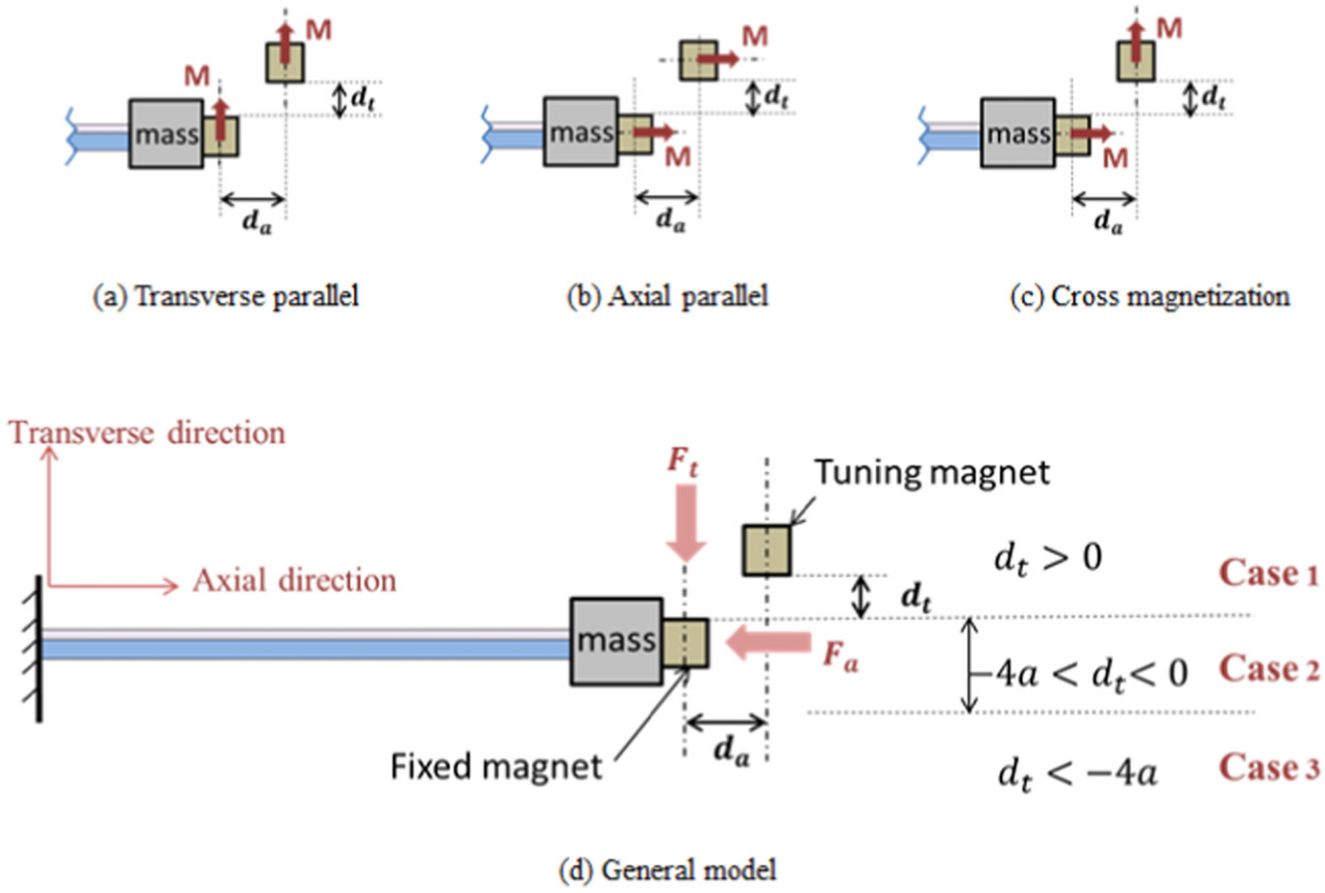

Figure 1. A schematic of the 2D resonant frequency tuning approach. (a) Transverse parallel magnetization orientation; (b) axial parallel magnetization orientation; (c) cross magnetization orientation; (d) general model.

Table 1. The parameters of the multilayer laminated cantilever beam and magnets used for the analysis.

Symbol	Description	Value	Units
	Cantilever beam		
w	Width	1×10^{-3}	m
L	Length	10×10^{-3}	m
t_p	Thickness of PZT layer	50×10^{-6}	m
t_s	Thickness of Si layer	100×10^{-6}	m
	Magnets		
$2a$	Side length of cuboidal magnet $(2a)^3$	0.5×10^{-3}	m
ρ_{mag}	Density (NdFeB)	7400	kg m^{-3}
μ_0	Air permeability	1.257×10^{-6}	H m^{-1}
M_0	Magnetization	0.796×10^{6}	A m^{-1}
	Tip mass		
a_t	Side length of cuboidal tip proof mass	1.0×10^{-3}	m
ρ_t	Density (Si)	2330	kg m^{-3}

parallel springs, with the transverse stiffness k_t and axial stiffness k_a denoted as variable springs which are a function of the transverse and axial applied magnetic forces, respectively, and the beam stiffness k_{beam} is a function of the material and geometry of the beam. Dampers b_m and b_e denote the mechanical and electrical damping, respectively, in the system.

Based on figure 2, the effective stiffness relating the external magnetic forces and the effective tuned frequency ω_{2D} of the cantilever beam in a 2D space can be expressed as shown in (1) and (2), where k_{eff} is the effective system stiffness and m_{eff} is the effective mass of the cantilever beam such that

$$k_{eff} = k_{beam} + k_t + k_a, \tag{1}$$

$$\omega_{2D} = \sqrt{\frac{k_{eff}}{m_{eff}}}. \tag{2}$$

When a transverse magnetic force is used to tune the resonant frequency of the cantilever beam [9], the transverse magnetic force (applied transverse to the beam) will result in a change in the transverse stiffness k_t and can be written as

$$k_t = -\frac{\partial F_t}{\partial d_t}. \tag{3}$$

On the other hand, when an axial tensile load is applied to the cantilever beam, it will increase the resonant frequency of the cantilever, while an axial compressive load decreases the resonant frequency. A formula for the resonant frequency

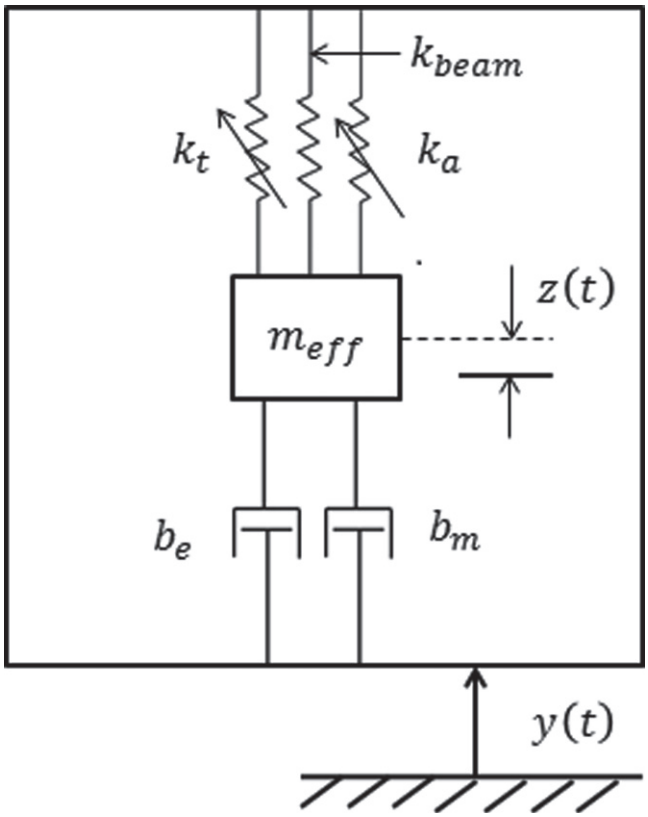

Figure 2. Lumped model of the 2D magnetic tuning approach, where the transverse and axial stiffnesses are represented as variable springs and are functions of the separation of the magnets in 2D space.

of a cantilever with an axial load F_a is given [12] as

$$\omega_a = \omega_{beam}\sqrt{1 + \frac{F_a}{F_b}}, \tag{4}$$

where ω_a is the resonance frequency with axial load, ω_{beam} is the original natural frequency of the beam, and F_b is the axial load required to buckle the beam (here we are neglecting the eccentric nature of the axial loading). Equation (4) shows that the frequency shift resulting from the axial force will be from a magnitude of zero (for the case where $F_a = -F_b$) to $\sqrt{2}$ times ω_{beam}, given that the axial force F_a must be less than the axial buckling load F_b. From (4), one can derive the expression for the axial stiffness term to be used in the calculation of the effective stiffness as shown in (1). Given an axial buckling load for a cantilever beam of $F_b = \frac{\pi^2 EI}{4L^2}$ [12], one can show that the axial stiffness k_a can be written as

$$k_a = \frac{12}{\pi^2 L}F_a, \tag{5}$$

where the axial stiffness k_a is only a function of the geometric parameters of the beam and the axial load F_a.

2.3. Magnetic tuning forces

According to (3) and (5), the transverse stiffness k_t is a function of magnetic transverse force F_t and the axial stiffness k_a is related to the axial load F_a, respectively. Here a three-dimensional (3D) analytical calculation of the forces exerted between two cuboidal magnets developed by Yonnet [13] is utilized based on the gradient of interaction energy. From [13], the magnetic forces between the fixed magnet and the tuning magnet can be written as

$$F = \frac{\mu_0 M_0^2}{4\pi}\sum_{i=0}^{1}\sum_{j=0}^{1}\sum_{k=0}^{1}\sum_{l=0}^{1}\sum_{p=0}^{1}\sum_{q=0}^{1}(-1)^{i+j+k+l+p+q} \times \phi(u_{ij}, v_{kl}, w_{pq}, r), \tag{6}$$

where

$$u_{ij} = ((-1)^j - (-1)^i)\cdot a \tag{7}$$

$$v_{kl} = ((-1)^l - (-1)^k)\cdot a + d_a \tag{8}$$

$$w_{pq} = ((-1)^q - (-1)^p + 2)\cdot a + d_t \tag{9}$$

$$r = \sqrt{{u_{ij}}^2 + {v_{kl}}^2 + {w_{pq}}^2} \tag{10}$$

and the function ϕ is dependent on whether the transverse or axial force is of interest, such that

$$\phi = -uw\ln(r-u) - vw\ln(r-v) + uv\tan^{-1}\frac{uv}{rw} - rw \quad (\text{for } F_t), \tag{11}$$

$$\phi = \frac{1}{2}(u^2 - w^2)\ln(r-u) + uv\ln(r-u) + uw\tan^{-1}\frac{uv}{rw} + \frac{1}{2}rv \quad (\text{for } F_a). \tag{12}$$

Based on the expressions above, it is clear that in 2D space, both the transverse force F_t and axial force F_a are related to the separation distances between the magnets (d_t and d_a) as shown in figure 1, such that a single position (d_a, d_t) of the tuning magnet introduces both transverse force F_t and axial force F_a in the system. The contact force between two magnets is defined as the force of attraction with zero axial and transverse gaps (i.e. $d_a = 2a$, $d_t = -2a$) and can be calculated using the unwieldy equation provided in [14]. This contact force F_0 is used to normalize the transverse and axial forces in the discussion below.

To verify the analytical results obtained using the expressions above, COMSOL magnetostatics 3D model with AC/DC module was used to simulate the magnetic forces between the fixed magnet and the tuning magnet. Specifically, the COMSOL simulation is based on the assumption of ideal magnets with a relative permeability of 1 and a remanent magnetization of $\mu_0 M_0 = 1$ T. The boundary conditions in the model include air surrounding the two cuboidal magnets with a permeability of 1.257×10^{-6} H m^{-1} as given in table 1. In addition, a fine mesh is used in the domain of the magnets to provide an accurate magnetic force computation. Once the magnetic flux field is calculated, a stationary study using COMSOL is then used to determine the transverse and axial forces due to the relative locations of the magnets in 2D space.

2.4. Constraints

In order to avoid damage to the cantilever beam in operation, dynamic failure due to the yield, buckling, and fatigue, respectively, must be avoided. The first limitation is that the stress generated from the applied transverse and axial forces is not greater than the yield stress of any component of the beam. The dynamic stress is the stress caused by the vibration of the beam and can be calculated by using the adapted static analysis, where the stress in the beam is due to the application of a force of magnitude F_{tip} at a distance L from the fixed end of the beam [15]. On the other hand, buckling is a failure mode that may result from an axial force applied by the tuning magnet, such that the maximum applied axial force to the cantilever beam is limited by the buckling force $F_{\text{b}} = \frac{\pi^2 EI}{4L^2}$ (here we neglect the eccentric offset nature of the applied axial load in the case where the magnets are not aligned along the axis of the cantilever beam).

Lastly, if one wishes to account for the long-term behavior of the system, then one must also account for fatigue, such that the fatigue stress (which is always less than or equal to the failure stress) should more appropriately be used in the analysis. The fatigue stress is the value of stress at which failure occurs after N_{f} cycles of cyclic loading. For an energy harvester, fatigue could result in a decrease in either the piezoelectric properties or mechanical properties of the system. For example, based on results from the literature [16], the fatigue stress for PZT ceramics based on S–N curves (stress amplitude versus number of cycles) at 10^5 cycles is given as $\sigma_{\text{fatigue}} = 55$ MPa, whereas the failure stress at the zero-cycle (not accounting for fatigue) given as $\sigma_{\text{failure}} = 80$ MPa.

Therefore, despite the simplified vision of a limitless lifetime source of electrical energy, in actuality the long-term fatigue performance of the continuously vibrating cantilever beam will be a factor that must be considered under real-life operating conditions for energy harvesting devices. For the sake of simplicity, in the sections below the results obtained for the normalized magnetic forces and the theoretical tuned frequencies of the cantilever beam are shown for a wide range of magnet positions; however, some of these positions may result in damage to the cantilever based on the constraints outlined above. For practical implementation, a more detailed consideration of the impact of the stresses generated within the vibrating beam as a function of these external applied magnetic forces would need to be considered.

3. Results and discussion

Using the approach outlined above, one can examine the resulting transverse and axial components of the magnetic force, their contributions to the effective system stiffness, and the overall change in resonant frequency of the cantilever beam as a function of the location of the tuning magnet in 2D space. In addition, as shown in figure 1, the 2D tuning approach can be analyzed for three different cases of the magnetization orientations (transverse parallel, axial parallel, and cross magnetization direction) which will be discussed separately below. The simulation results obtained for the magnetic transverse and axial forces based on COMSOL magnetostatics 3D model verified the theoretical calculations performed by MATLAB. These magnetic forces can then be related to the stiffness contributions and change in resonant frequency based on the approach described in section 2. Although there are three different possible magnetization orientations with respect to the arrangement of the magnets, the magnetic forces of the transverse and axial parallel magnetizations are identical, with the only difference being the manner that the force is applied to the cantilever beam [13] as discussed in section 3.1.1. Section 3.1.2 discusses the impact of these magnetic forces on the stiffness and resonant frequency for the transverse parallel magnetization orientation, while sections 3.2 and 3.3 extend this analysis for the axial parallel and cross magnetization orientations, respectively.

3.1. Tuning with transverse parallel magnetization orientation

Here the results for the transverse parallel magnetization orientation (figure 1(a)) are presented including both theoretical calculations and simulations for magnetic tuning forces. In the following discussion, the tuning magnet is assumed to always be to the right side of the fixed magnet such that $d_{\text{a}} > 0$. Based on the location of the tuning magnet, there are three cases to be considered: case (1) when the tuning magnet is above the tip magnet, i.e. $d_{\text{t}} > 0$; case (2) when the tuning magnet and tip magnet are partially (or fully) overlapped in the transverse direction such that $-4a < d_{\text{t}} < 0$, specifically for this case the physical system requires that $d_{\text{a}} > 2a$; and case (3) when the tuning magnet is below the tip magnet on the cantilever beam such that $d_{\text{t}} < -4a$ as shown in figure 1(d). In addition to the magnetic forces observed as a result of the relative magnet location, the effects of stiffness (transverse stiffness and axial stiffness) and net tuning frequency changes are further detailed below to illustrate this 2D tuning method.

3.1.1. Tuning forces versus position. The analytical calculations for the tuning magnetic transverse force F_{t} and axial force F_{a} are implemented in MATLAB using (6) to (12) assuming discrete movement of the magnet in 2D space such that $d_{\text{a}} = (0\text{a}: 0.5\text{a}: 5\text{a})$ and $d_{\text{t}} = (0.5\text{a}: 0.5\text{a}: 5\text{a})$, where a refers to half edge the cuboidal magnet, which is assumed to be equal for both magnets for simplicity. The analytical calculations are verified using COMSOL as described previously.

Figure 3(a) shows the normalized transverse force with respect to the normalized transverse displacement, where forces are normalized with respect to the contact force F_0 and displacements are normalized with respect to the magnet half edge length a. It is clear that the theoretical results from MATLAB match well with the COMSOL simulation results. Based on the results from figure 3(a), when $d_{\text{a}} = 0$ and $d_{\text{a}} = 1a$, the tuning transverse force is decreasing with increasing transverse displacement d_{t}, while if d_{a} is much

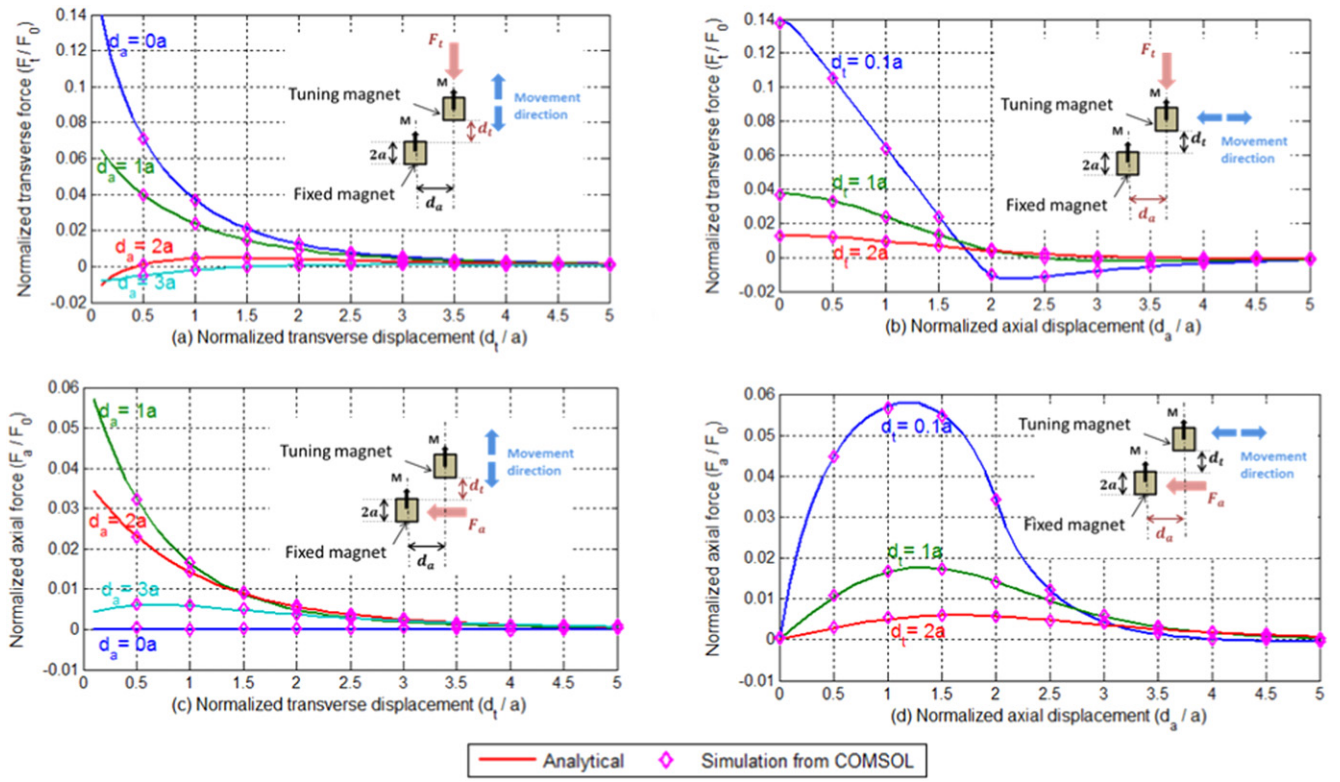

Figure 3. Transverse parallel magnetization orientation for $\boldsymbol{d_t} > 0$: (a) transverse force versus transverse displacement; (b) transverse force versus axial displacement; (c) axial force versus transverse displacement; (d) axial force versus axial displacement. Forces are normalized with respect to the contact force $\boldsymbol{F}_0$ and displacements are normalized with respect to the magnet half edge size a.

greater than zero, for instance, $d_a = 2a$ and $d_a = 3a$ the transverse force is very small and in some cases may be slightly less than zero. This is due to the fact that for larger d_t, the larger separation distance alters the magnetic flux lines in a manner which can impact the direction of the applied magnetic force, although the magnitude of the force as these separation distances increase is very small. As expected, figure 3(b) shows that the transverse force is largest at zero axial displacement ($d_a = 0$) and decreases with increasing axial displacement d_a. For the curve of $d_t = 0.1a$, the transverse force decreases through a value of zero before going slightly negative at larger axial displacements before trending towards zero, again illustrating the complexity of the magnetic field at larger separation distances. This is a characteristic observed in both the analytical solution and the COMSOL simulations, which show excellent agreement. Clearly the transverse force in 2D space is a function of both transverse and axial displacements.

The magnetically-induced axial forces with respect to both the normalized transverse and axial displacements are illustrated in figures 3(c) and (d) for the case where $d_t > 0$. In figure 3(c), the axial magnetic force decreases to zero as the transverse displacement d_t increases, with a slight maximum observed in the curve for $d_a = 3a$. Figure 3(d) illustrates that the axial force will increase to a maximum value at some axial displacement, after which it decreases to zero for larger axial displacements, with excellent agreement again observed for the analytical and COMSOL results.

The second case to be analyzed is when the tuning and tip magnets are partially (or fully) overlapped in the transverse direction such that $-4a < d_t < 0$. The transverse and axial magnetic forces obtained from the analytical and COMSOL solutions are shown in figure 4. As discussed in [17], when the transverse displacement $d_t = -2a$, the magnets are perfectly overlapped in the transverse direction and the solution is not well-defined; thus, a transverse displacement $d_t = -1.9a$ is used. As expected, figure 4 illustrates that both transverse and axial forces approach zero for larger axial displacements.

The third case for analysis is when the tuning magnet is fully below the fixed magnet such that $d_t < -4a$. Because the magnetic field of an ideal cuboidal magnet is symmetric, the induced magnetic forces are also symmetric. Both analytical and simulation results show that the transverse and axial forces can be expressed as $F_t(d_t) = -F_t(-4a - d_t)$ and $F_a(d_t) = -F_a(-4a - d_t)$. Therefore, compared to the transverse and axial forces in the first case ($d_t > 0$), those in the third case ($d_t < -4a$) will have the same magnitude of the force but in the opposite direction and thus are not repeated here.

3.1.2. Impact of tuning forces on effective stiffness and resonant frequency. As discussed in section 2, magnetic forces which are a function of the position of the tuning magnet contribute to changes in the transverse and axial stiffness of the cantilever beam. These changes in stiffness

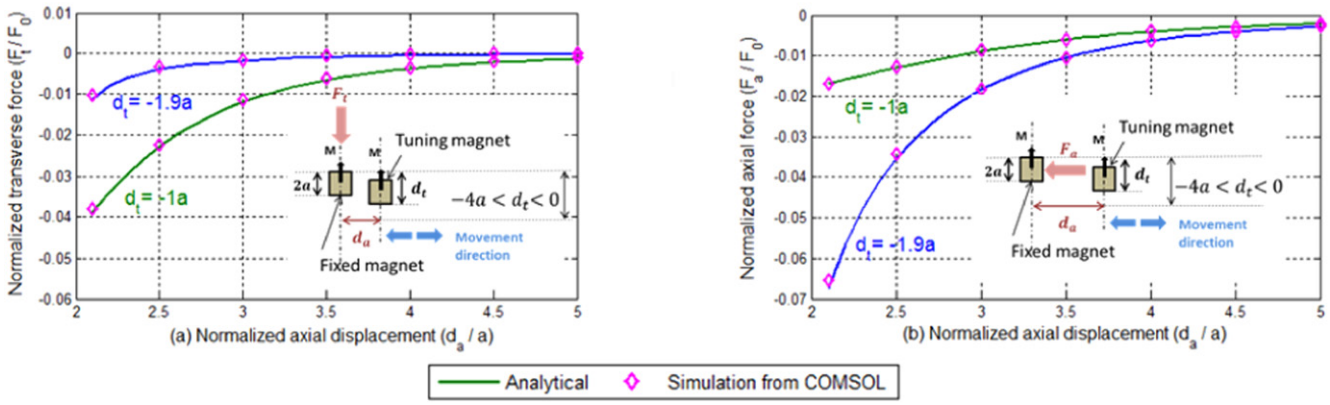

Figure 4. Normalized magnetic tuning forces with respect to the normalized tuning magnet positions where $-4\boldsymbol{a} < \boldsymbol{d_t} < 0$. (a) Transverse force versus axial displacement; (b) axial force versus axial displacement.

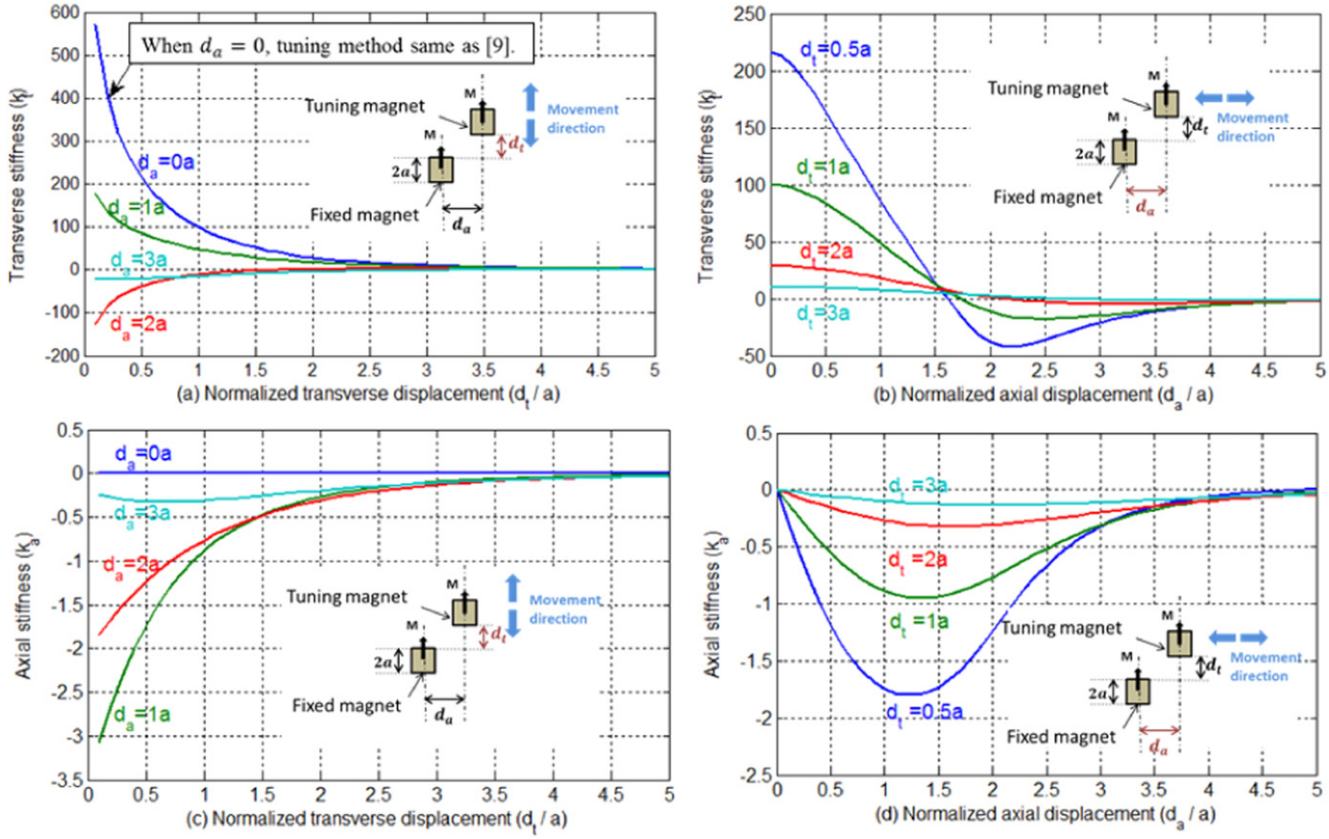

Figure 5. Transverse and axial stiffness for transverse parallel magnetization orientation of magnets where $\boldsymbol{d_t} > 0$ (a) transverse stiffness versus transverse displacement; (b) transverse stiffness versus axial displacement; (c) axial stiffness versus transverse displacement; (d) axial stiffness versus axial displacement. Displacements are normalized with respect to the magnet half edge size a.

directly contribute to the effective frequency of the cantilever beam as shown in (1) and (2). Given the determination of the magnetic forces above, it is thus straightforward to determine the transverse and axial stiffness terms as a function of tuning magnet location using (3) and (5), respectively, as shown in figures 5 and 6. It is clear from these figures that the magnitude of the transverse stiffness is much larger than the contribution of the axial stiffness for this transverse parallel magnetic orientation. In addition, as shown in figure 5(a), when $d_a = 0$ the magnets are aligned and the relative motion of the tuning magnet is purely transverse to the cantilever, which is equivalent to the tuning approach described previously in the literature [9]. In addition, figure 5(b) shows that the transverse stiffness is largest at zero axial displacement $d_a = 0$ and decreases with increasing axial displacement. A characteristic observed for the curves of $d_t = 0.5a$, $d_t = 1a$ and $d_t = 2a$ is that the transverse stiffness decreases through zero before again approaching zero at

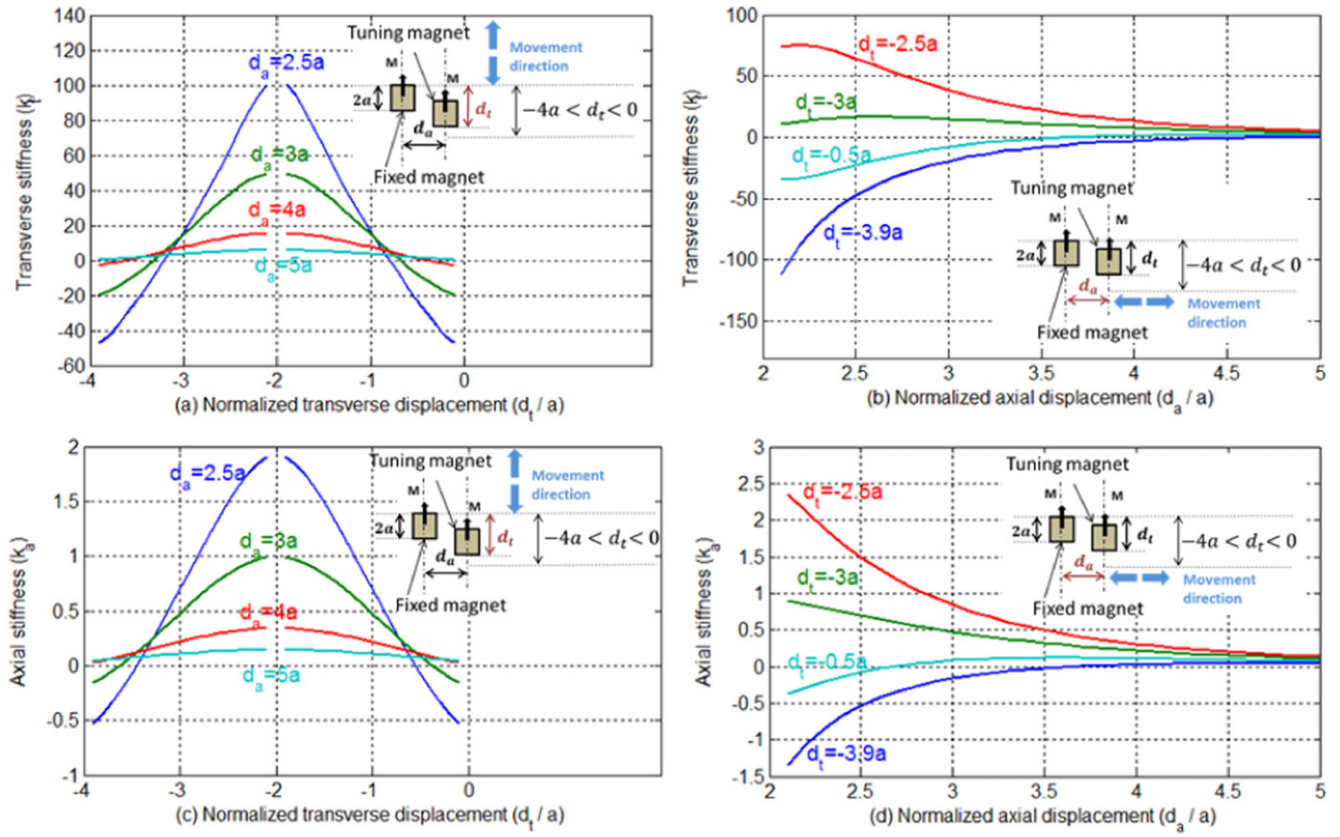

Figure 6. Transverse and axial stiffness for transverse parallel magnetization orientation of magnets where $-4\boldsymbol{a} < \boldsymbol{d_t} < 0$ (a) transverse stiffness versus transverse displacement; (b) transverse stiffness versus axial displacement; (c) axial stiffness versus transverse displacement; (d) axial stiffness versus axial displacement. Displacements are normalized with respect to the magnet half edge size a.

larger axial displacements, illustrating the complexity of the magnetic fields in 2D space.

When the cantilever beam is subjected to an axial force, an axial stiffness is introduced which alters the resonant frequency of the cantilever beam. The axial stiffness k_a as given in (5) is only a function of the geometry of the beam and the axial load F_a. Based on section 2.2, figures 5(c) and (d) show the variation of axial stiffness k_a with respect to the normalized axial and transverse displacements of the tuning magnet when $d_t > 0$. In this case, a compressive load is applied between the two magnets and the induced axial stuffiness k_a is negative such that $k_a < 0$, with the effective stiffness of the beam decreasing according to (1). Figure 5(d) shows that the axial stiffness will decrease to a minimum value at some axial displacement, after which it increases to zero for larger axial displacements. This characteristic is consistent with the results of the axial forces shown in figure 3(d).

Due to symmetry, for case 3 (when the tuning magnet is fully below the fixed magnet such that $d_t < -4a$), the analysis of the axial and transverse stiffnesses will follow figure 5 and thus is not repeated here. For case 2, according to the theoretical magnetic force equations [17], the results for a transverse displacement $d_t = -2a$ are ill defined (resulting in the gaps shown in figures 6(a) and (c)). However, the results of stiffness in figures 6(a) and (c) suggest that both transverse stiffness and axial stiffness are symmetric about $d_t = -2a$ and will reach a maximum value when the transverse displacement approaches $-2a$, where the two magnets are aligned in the axial direction. In addition, as expected, figures 6(b) and (d) illustrate that both transverse and axial stiffnesses approach zero for larger axial displacement. Note that when the tuning magnet and tip magnet are partially (or fully) overlapped in the transverse direction such that $-4a < d_t < 0$ (in case 2), the axial stiffness is not always negative (as was observed for case 1) as shown in figure 6(d). Lastly, as shown in figure 6(d), when $d_t = -2.5a$ and $d_t = -3a$ the axial stiffness $k_a > 0$. In this case, a tensile load will be applied to the cantilever beam such that $F_a > 0$, which will result in an increase in the resonant frequency.

When both transverse and axial magnetic forces are simultaneously applied on a clamped-free cantilever beam, the effective resonant frequency is altered as the result of both transverse stiffness and axial stiffness contributions to the overall effective stiffness of the system as shown in (1). To illustrate the impact of magnet location on the resonant frequency of the system, a contour plot of the change in resonant frequency as a function of tuning magnet position in 2D space is shown in figure 7 for the transverse parallel magnetization orientation. Here we assume that movement of the tuning magnet can be described as $d_a = (0a\text{: } 0.5a\text{: } 5a)$ and $d_t = (0.5a\text{: } 0.5a\text{: } 5a)$, with the tuning step defined as $0.5a$. (However, note that the tuning magnet positions should be subject to the appropriate constraints for the cantilever

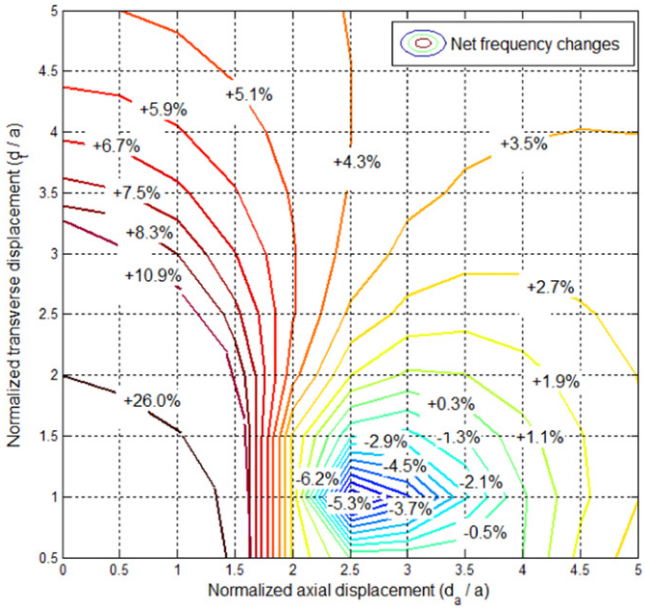

Figure 7. Contour plot of net resonant frequency changes of magnetically tuned cantilever beam for transverse parallel magnetization orientation of the magnets.

beam as outlined in section 2.4.) Given the transverse parallel magnetization orientation being considered here, the axial forces are in general relatively small and do not drastically shift the resonance of the beam. For the specific parameters listed in table 1, the untuned frequency of the cantilever beam is 417.8 Hz and the projected tuning range is between -6.2% to $+26\%$, which corresponds to 391.9–526.5 Hz.

3.2. Tuning with axial parallel magnetization directions

A second scenario to be analyzed is when the two magnets are aligned with the magnetization orientations in the axial parallel direction as shown in figure 1(b). Again both the transverse force F_t and axial force F_a as a function of axial (d_a) and transverse (d_t) location of the tuning magnets can be found using the approach described in section 2.3; as discussed previously, these are directly related to the forces shown in figures 3 and 4 above for the transverse parallel orientation. These forces again contribute to the magnetic transverse stiffness k_t and the axial magnetic stiffness k_a of the system, which impact the net effective resonant frequency of the system as shown in (1) and (2).

As we assume that the tuning magnet is always moving to the right of the fixed magnet such that $d_a > 2a$, figure 8 shows the variation of transverse stiffness k_t and axial stiffness k_a with respect to normalized displacements of the tuning magnet. For case 1 and case 3, when $d_t > 0$ or $d_t < -4a$, the transverse stiffness and axial stiffness with respect to the normalized transverse displacement follow the same symmetric relationship described previously. When the tuning magnet and tip magnet are partially (or fully) overlapped in the transverse direction such that $-4a < d_t < 0$ (case 2), the axial stiffness k_a is always negative. Note that in figures 8(b) and (d), values of $d_a < 2a$ would result in overlap of the magnets and are not considered. Specifically, it is clear from figure 8 that both transverse stiffness and axial stiffness will attain the maximum absolute value when the two magnets are aligned in the axial direction where $d_t = -2a$ such that the 2D tuning model simplifies to the 1D horizontal tuning approach described previously in the literature [10]. In addition, figure 8 also illustrates that the transverse stiffness term is significantly larger than the axial stiffness for the 2D tuning scenario with the axial parallel magnet orientation. Also note that the magnitudes of the transverse stiffness in the axial parallel orientation are, as expected, much smaller than those obtained for the transverse parallel orientation of the magnets as shown in figure 5(a).

A contour plot of frequency differences obtained using the 2D magnetic tuning with an axial parallel magnetization orientation is shown in figure 9, assuming a tuning magnet range of $d_a = (2a: 0.5a: 5a)$ and $d_t = (0a: 0.5a: 5a)$. As shown in figure 9, a tuning range of 71.1 Hz (434.5–505.6 Hz) for axial parallel magnetization is obtained, with the corresponding frequency differences between 4% to 12.1% of the unturned frequency. Note that in the assumed 2D tuning space, the tuning frequencies are always larger than the untuned frequency due to the assumption that the tuning magnet is always above and on the right side of the fixed magnet. Obviously as the tuning magnet is further removed from the cantilever beam the impact of the applied magnetic forces would decrease and the tuned frequency approaches the untuned frequency of the system.

3.3. Tuning with cross magnetization orientation

Similar to the approach used above, the tuning performance of the system for the cross magnetization orientation direction as shown in figure 1(c) is highlighted below.

3.3.1. Tuning forces versus positions. For the cross magnetization orientation, theoretical calculations performed by MATLAB and simulation results by COMSOL magnetostatic 3D model in AC/DC module are given in figure 10. Excellent agreement for the calculated forces is again observed using these two approaches. Because of the cross magnetic orientation of the magnets, one difference that is observed from previous magnetic orientations is that the largest transverse forces F_t are not obtained when the magnets are aligned and $d_a = 0$ (see figure 10(b)). As discussed before, this results from the complex magnetic fields generated as the tuning magnetic is moved in 2D space. Figures 10(c) and (d) describe the normalized axial forces versus normalized transverse and axial displacements, respectively. As might be expected, a comparison of figures 3 and 10 shows that the magnitudes of the magnetic forces are much smaller for the cross magnetization direction.

3.3.2. Impact of tuning forces on effective stiffness and resonant frequency. By applying the effective stiffness theory, the impact of these magnetic forces on the contributions to the effective stiffness can be calculated as shown in figure 11. Compared to the effective stiffness

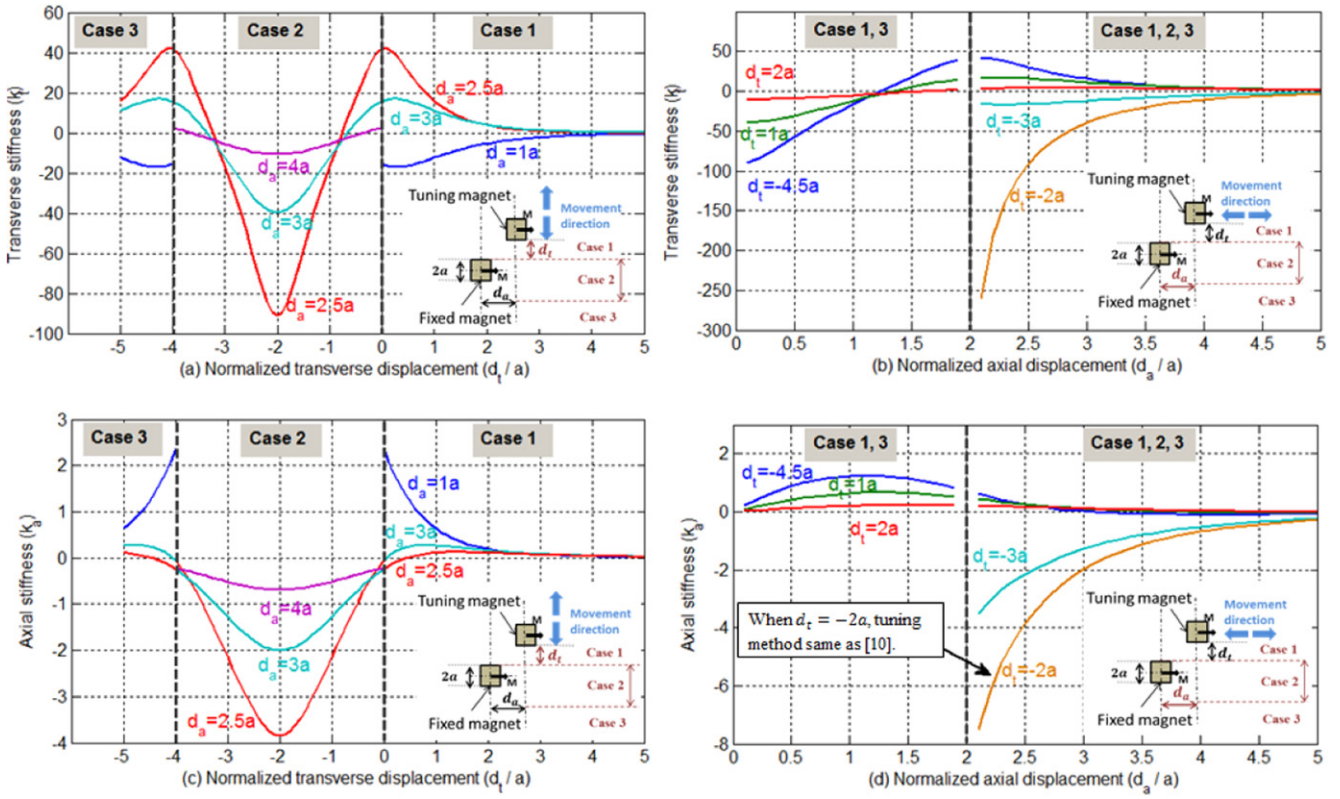

Figure 8. Transverse and axial stiffness for axial parallel magnetization orientation of magnets. (a) Transverse stiffness versus transverse displacement; (b) transverse stiffness versus axial displacement; (c) axial stiffness versus transverse displacement; (d) axial stiffness versus axial displacement. Displacements are normalized with respect to the magnet half edge size a.

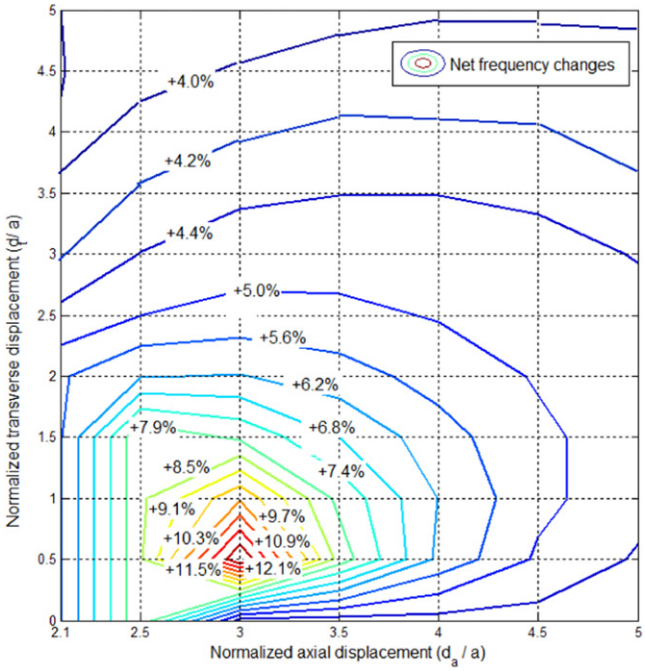

Figure 9. Contour plot of net frequency changes of tuning for axial parallel magnetization for $0 < \boldsymbol{d_t} < 5\boldsymbol{a}$ and $2.1\boldsymbol{a} < \boldsymbol{d_a} < 5\boldsymbol{a}$.

contributions found for the transverse parallel (figure 5) and the axial parallel (figure 8) magnetic orientations, we see that the cross parallel magnetization results in a somewhat lower transverse stiffness contribution and similar axial stiffness values compared to the transverse parallel orientation, with the largest contributions to the axial stiffness found for the axial parallel orientation.

In addition, a contour plot of frequency differences obtained using the 2D magnetic tuning with a cross parallel magnetization orientation assuming a tuning magnet range of $d_{\mathrm{a}} = (2a\text{: } 0.5a\text{: } 5a)$ and $d_{\mathrm{t}} = (0a\text{: } 0.5a\text{: } 5a)$ is shown in figure 12. For the given 2D tuning space, figure 12 shows that for the cross magnetization orientation effective resonant frequencies between −1.4% to +23.3% of the untuned system frequency, corresponding to 412.0–514.5 Hz, can be obtained for this system.

4. Case study

A simple experimental study measuring the effective resonant frequency of a 2D magnetically tuned cantilever beam energy harvester was conducted to confirm the results from the analytical and computational models described above. Here the transverse parallel magnetic orientation, which was found to be the most effective way to implement the 2D tuning approach as discussed in section 3, is implemented to illustrate this tuning approach. As shown in figure 13, the prototype consisted of a cantilever beam, a tip magnet, a tuning magnet, and a housing frame which is mounted on a shaker to provide a given vibration of known amplitude and frequency. The cantilever beam is a piezoelectric stripe actuator (APC

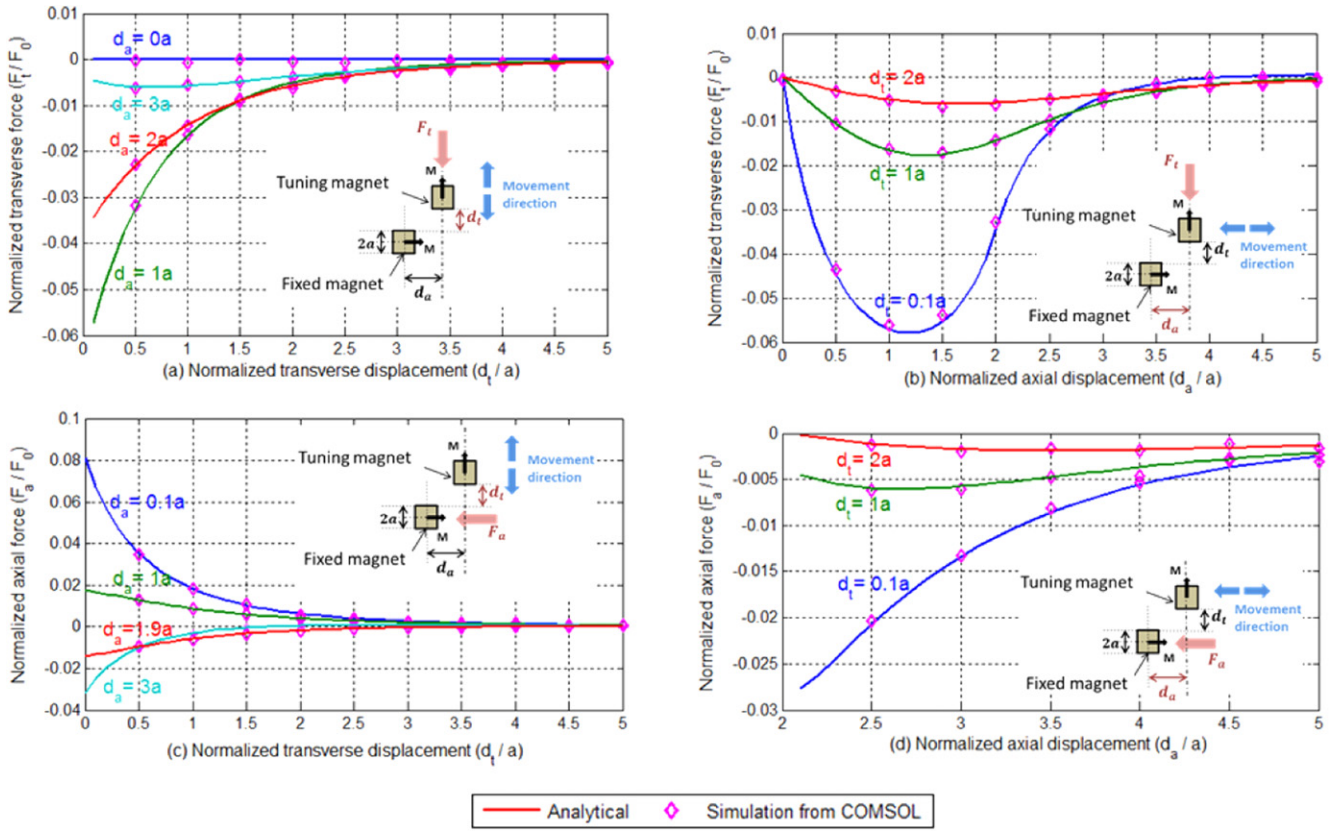

Figure 10. Normalized forces for cross magnetization orientation where $\boldsymbol{d_t} > 0$: Transverse force versus transverse displacement; (b) transverse force versus axial displacement; (c) axial force versus transverse displacement; (d) axial force versus axial displacement. Forces are normalized with respect to the contact force $\boldsymbol{F}_0$ and displacements are normalized with respect to the magnet half edge size a.

International Ltd, Model 40-2010), and all necessary dimensions and properties are listed in table 2.

In the experimental configuration, the entire housing of the energy harvester is fixed to a shaker (Model 4810 from Bruel & Kjaer) which is used to provide a known vibration input excitation to the system using a function generator (HP 4120 series) with a power amplifier (Bruel and Kjaer). Within the energy harvesting device, the cantilever beam with a fixed magnet at the tip is vibrating in the vertical direction, with two tuning screws for the transverse and axial directions, respectively, used to carefully adjust the location of the tuning magnet in 2D space with respect to the fixed magnet. The pitch of the screws and the number of turns are used to determine the displacement in both transverse and axial directions. For the current configuration, the transverse tuning displacements are from 2.54 to 15.24 mm while the axial tuning displacements are between 0 and 10.16 mm, with 2.54 mm steps in both transverse and axial directions corresponding to the half-length of the magnets. The real time voltage output from the piezoelectric stripe actuator is collected using a data acquisition (DAQ) card (National Instruments, model NI USB-6009) and LabView software. By adjusting the different relative positions between the magnets in 2D space, the resonance of the tuned system was determined based on measuring the frequency of the peak voltage obtained for a given location.

The values obtained for the experimentally tuned frequencies as a function of magnet position for the case of the transverse parallel magnetization orientation are given in table 3. Within experimental error, we find that the cantilever beam system (untuned frequency of 61 Hz) can be tuned from approximately 51 to 87 Hz based on 2D tuning space explored in the table. The experimentally obtained results are further compared with the analytical calculations for the frequency differences are shown in table 4. Based on the geometry parameters of the beam and magnets listed in table 2, the experimental tuning range for transverse parallel magnetization of this prototype is between -16.2% to $+23\%$. As shown in table 4, the experimentally obtained frequencies in most cases closely match the analytical values, with significant error only found for the case of $d_a = 2a$, where the two magnets are aligned with each other in the axial direction. We attribute this error to the fact that the gradients of the magnetic force are largest when the magnets are aligned, such that the results in this case are particularly sensitive to positional errors in the experimental testing.

5. A note on power output

In general, an energy harvesting device can be modeled as a spring–mass–damper system as shown in figure 2, where the mechanical dashpot b_m accounts for the energy losses due to

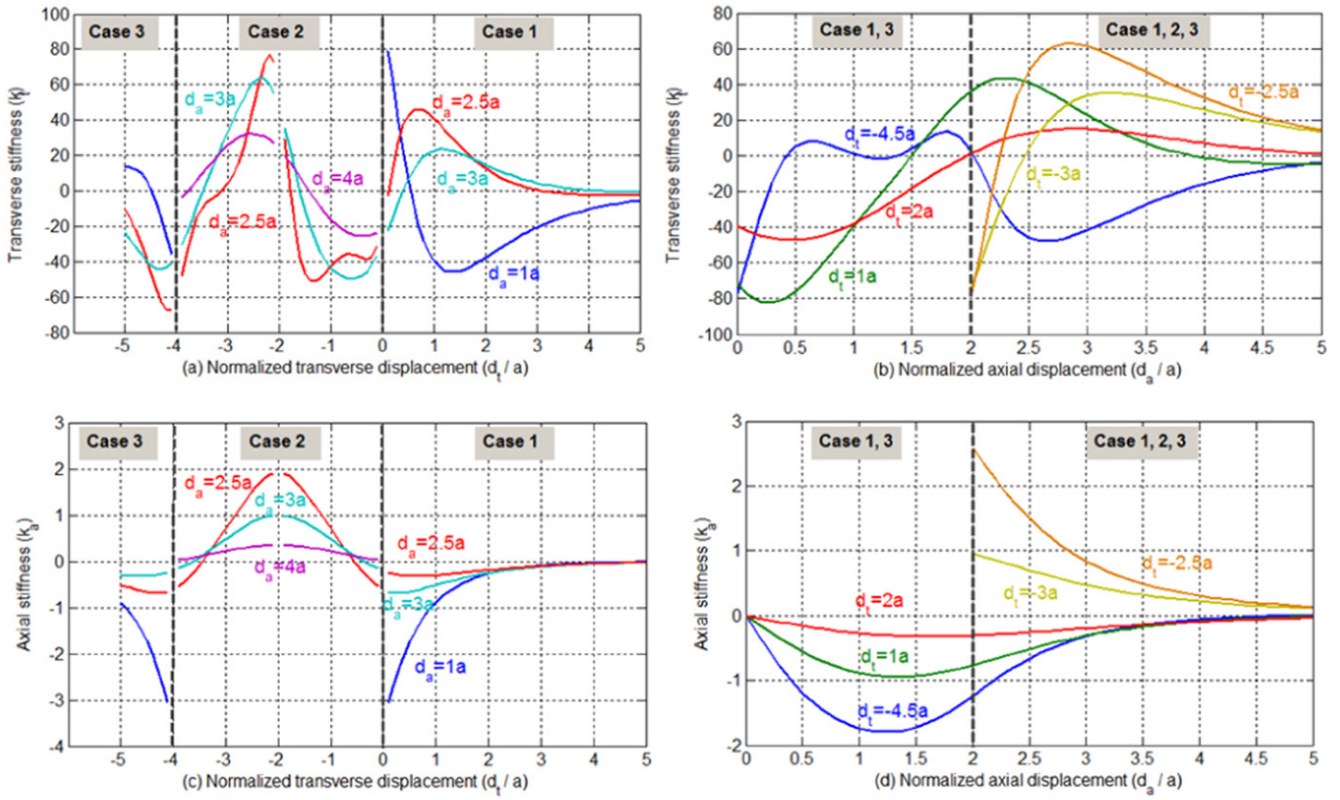

Figure 11. Transverse and axial stiffness for cross magnetization orientation of magnets. (a) Transverse stiffness versus transverse displacement; (b) transverse stiffness versus axial displacement; (c) axial stiffness versus transverse displacement; (d) axial stiffness versus axial displacement. Displacements are normalized with respect to the magnet half edge size a.

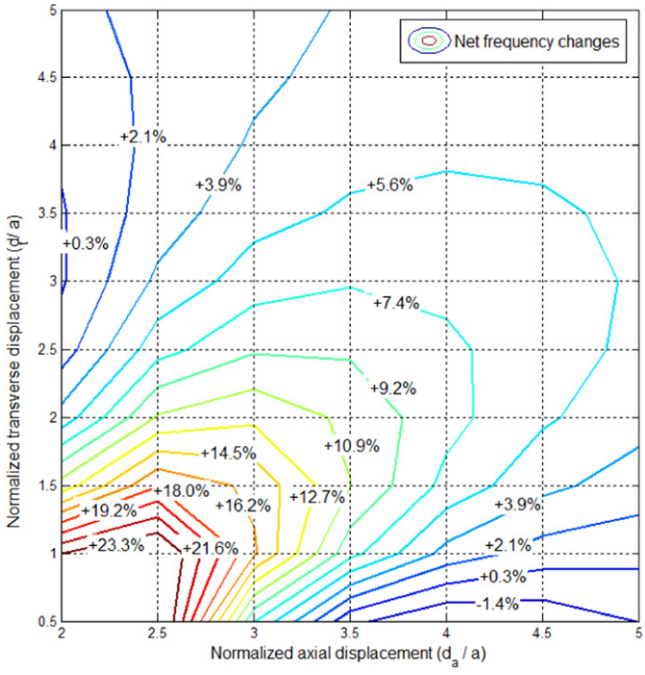

Figure 12. Contour plot of net frequency changes of tuning for cross magnetization orientation for $0.5\boldsymbol{a} < \boldsymbol{d_t} < 5\boldsymbol{a}$ and $2\boldsymbol{a} < \boldsymbol{d_a} < 5\boldsymbol{a}$.

structural and viscous damping, while the electrical damping b_e corresponds to the energy harvested through the energy conversion mechanism [11]. Given a sinusoidal excitation vibration $y(t) = Y \sin \omega_s t$, where Y and ω_s are the source

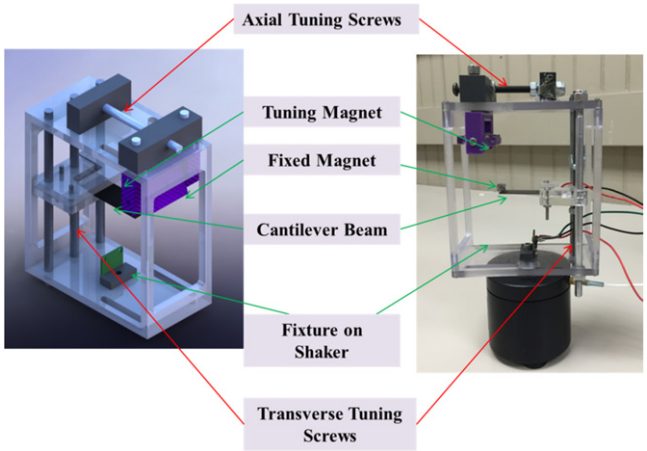

Figure 13. Schematic of 2D resonant frequency tuning approach: (left) model, (right) experimental setup.

vibration amplitude and frequency, respectively, the net electrical power generated can be written as [11]

$$P = \frac{m_{\text{struc}} \zeta_t Y^2 \left(\frac{\omega_s}{\omega_{\text{struc}}}\right)^3 {\omega_s}^3}{\left[1 - \left(\frac{\omega_s}{\omega_{\text{struc}}}\right)^2\right]^2 + \left[2\zeta_t \frac{\omega_s}{\omega_{\text{struc}}}\right]^2}, \tag{13}$$

where ζ_t is the total damping ratio ($\zeta_t = \zeta_m + \zeta_e$) which is the sum of mechanical damping ratio ζ_m and electrical damping ratio ζ_e and ω_{struc} is the undamped natural frequency of the

Table 2. The parameters of cantilever beam and magnets used in the experimental confirmation of the 2D magnetic frequency tuning approach. (Parameters not explicitly listed in table 2 are the same as those given in table 1.)

Description	Value	Units
Cantilever beam		
Width	20×10^{-3}	m
Length	60×10^{-3}	m
Thickness of piezoelectric stripe actuator	0.7×10^{-3}	m
Magnets		
Side length	5.08×10^{-3}	m
Density (NdFeB)	7400	kg m^{-3}

Table 3. Experimental tuned frequency (Hz) of the 2D tuning approach for transverse parallel magnetization orientation. The untuned frequency of the system was 61 Hz.

	Experimental tuned frequency (Hz)				
	d_a/a				
	0	1	2	3	4
d_t/a					
1	86.81	78.00	52.15	51.08	51.15
2	80.64	70.47	55.16	56.99	54.14
3	74.74	68.29	56.66	58.06	56.05
4	68.77	65.09	56.98	59.98	57.61
5	65.16	63.43	56.94	60.72	59.94
6	64.49	61.68	57.62	61.94	60.60

vibrating structure. When the energy harvesting device is in resonance such that $\omega_s = \omega_{struc}$, the power output at resonance P_{res} can be simplified as

$$P_{res} = \frac{\zeta_e}{4{\zeta_t}^2} m_{struc} Y^2 {\omega_s}^3. \quad (14)$$

According to (14), when the device is vibrating in resonance, the power output is dependent on the mass of structure, the amplitude and frequency of the source vibration, and the damping characteristics of the system. As the vibration amplitude and frequency are a function of the environmental vibration source and thus not design variables, at resonance the vibrating structure and damping parameters can be optimized to maximize the power output of the energy harvesting device.

In the application of the 2D magnetic resonance frequency tuning approach, tuning of the resonant frequency will affect the power output of the device by directly changing the resonant frequency of the harvester. Determination of the power output from a particular device could be measured following procedures used previously in the literature [9, 10]. However, note that from a systems perspective, the energy needed to implement the tuning mechanism (in this case, the movement of the tuning magnets) should be included in an overall analysis of the system performance [18].

6. Conclusions

Given the increasing interest in the development of wireless sensor networks, it is desired to make the sensors self-contained with their own renewable power supply. Moreover, recent advances in low-power sensor technology have reduced the power requirements of these sensor nodes to the level of several milliwatts [19, 20], such that it is becoming increasingly feasible to implement self-powered wireless sensors. One such promising solution pursued here is vibration-based energy harvesting, which converts ambient (mechanical) vibration energy to electrical energy. Clearly, the energy harvesting power solution is preferable to batteries in terms of less maintenance and longer operational lifetime when compared to batteries and other chemical sources. However, a vibration-based energy harvester produces maximum power only when its resonant frequency is properly tuned with the environmental vibration frequency. As has been discussed in the literature, practical implementation of these harvesters will almost certainly require a way to tune the resonant frequencies to enable the device to harvest energy in various environments. In earlier work, a horizontal method to tune the frequency of energy harvester has been proposed [10]; this approach may be optimal at the MEMS scale since it is much more difficult to move the magnets vertically at that length scale.

In the current work a 2D magnetic stiffness tuning method, where the tuning magnet is free to move in 2D space with respect to the fixed magnet on the cantilever beam energy harvesting element is presented. By applying magnetic forces in 2D space, the effective resonant frequency of the system is related to two additional stiffness components added to the untuned system. Here we have shown that the transverse and axial magnetic forces and related stiffness contributions can be accurately calculated based on theoretical calculations provided earlier in the literature [17], with the results confirmed using a COMSOL magnetostatic 3D model. In particular, as the optimal magnetic orientation of the magnets for the 2D tuning approach is not clear, we examined the three different possible magnetization orientations (transverse parallel, axial parallel, and cross magnetization directions) between the fixed and tuning magnets to examine the effect of magnetic orientation on tuning. After analyzing these three different magnetization orientation directions, we conclude that the transverse parallel orientation may be the most effective in most cases as it provides the largest frequency bandwidth for the tuned harvester. In all cases, the transverse stiffness term is in general significantly larger than the axial stiffness contribution, suggesting that from a tuning perspective it may be possible to use the transverse and axial stiffness contributions for coarse and fine frequency tuning, respectively. Lastly, an experimental case study for the transverse parallel magnetization orientation verified the proposed model for the 2D resonant frequency tuning approach.

This 2D resonant frequency tuning approach extends earlier 1D approaches and may be useful, in particular, for applications where space constraints impact the available design space of the energy harvester. On the other hand, we note that a limitation of the proposed 2D tuning approach is that it will be more difficult than 1D solutions to practically implement, given the need to

Table 4. Comparison of analytical calculations and experimental data for the effective resonant frequency for transverse parallel magnetization orientation.

Comparison of analytical and experimental frequency (%)					
	d_a/a				
	0	1	2	3	4
d_t/a					
1	2.4%	0.9%	15.2%	−1.5%	−7.7%
2	−1.0%	1.7%	13.1%	0.2%	0.1%
3	−1.4%	0.8%	11.3%	3.1%	2.8%
4	1.3%	2.5%	10.5%	1.9%	3.1%
5	2.8%	2.7%	10.1%	1.5%	0.8%
6	1.1%	3.8%	8.4%	−0.3%	0.5%

accurately locate the tuning magnet in 2D space. In addition, because the same effective stiffness can correspond to multiple positions of the tuning magnet in 2D space, a tuning path which accounts for the energy costs associated with the tuning step and projected future frequency tuning requirements would be necessary to determine the final optimal tuning magnet position for adaptive, real-time tuning of the resonant frequency of the energy harvesting device [18]. Nonetheless, the proposed 2D tuning results may find use as a means of tuning the resonant frequency of vibration-based energy harvesting devices.

Acknowledgments

The authors acknowledge the assistance with modeling and experiments provided by undergraduate students Henry Hernandez, Jeffrey Paine, Thomas Battaglia, and Daniel Kamieniecki, who were supported by the Stevens Summer Scholars Program.

References

[1] Bult K, Burstein A, Chang D, Dong M and Fielding M 1996 A distributed, wireless MEMS technology for condition based maintenance *Integrated Monitoring, Diagnostics and Failure Prevention Conf., Society of Machine Failure Protection (Mobile, AL, USA)*

[2] Lynch J P, Sundararajan A, Law K H, Sohn H and Farrar C R 2005 Design of a wireless active sensing unit for localized structural health monitoring *Struct. Control Health Monit.* **12** 405–23

[3] Aygün B and Gungor V C 2011 Wireless sensor networks for structure health monitoring: recent advances and future research directions *Sensor Rev.* **31** 261–76

[4] Hudak N S and Amatucci G G 2008 Small-scale energy harvesting through thermoelectric, vibration, and radiofrequency power conversion *J. Appl. Phys.* **103** 101301

[5] Beeby S P, Tudor M J and White N M 2006 Energy harvesting vibration sources for microsystems applications *Meas. Sci. Technol.* **17** R175–95

[6] Zhu D, Tudor M J and Beeby S P 2010 Strategies for increasing the operating frequency range of vibration energy harvesters: a review *Meas. Sci. Technol.* **21** 022001

[7] Yao J J and MacDonald N C 1995 A micromachined, single-crystal silicon, tunable resonator *J. Micromech. Microeng.* **5** 257–64

[8] Leland E S and Wright P K 2006 Resonance tuning of piezoelectric vibration energy scavenging generators using compressive transverse preload *Smart Mater. Struct.* **15** 1413–20

[9] Challa V R, Prasad M G, Shi Y and Fisher F T 2008 A vibration energy harvesting device with bidirectional resonance frequency tunability *Smart Mater. Struct.* **17** 015035–45

[10] Zhu D, Roberts S, Tudor M J and Beeby S P 2010 Design and experimental characterization of a tunable vibration-based electromagnetic micro-generator *Sensors Actuators* A **158** 284–93

[11] Williams C B and Yates R B 1996 Analysis of a micro-electric generator for microsystems *Sensors Actuators* A **52** 8–11

[12] Lesieutre G A and Davis C L 1997 Can a coupling coefficient of a piezoelectric device be higher than those of its active material *J. Intell. Mater. Syst. Struct.* **8** 859–67

[13] Akoun G and Yonnet J P 1984 3D analytical calculation of the forces exerted between two cuboidal magnets *IEEE Trans. Magn.* **20** 1962–4

[14] Agashe J S and Arnold D P 2008 A study of scaling and geometry effects on the forces between cuboidal and cylindrical magnets using analytical force solutions *J. Phys. D: Appl. Phys.* **41** 105001

[15] Challa V R, Prasad M G and Fisher F T 2009 A coupled piezoelectric-electromagnetic energy harvesting technique for achieving increased power output through damping matching *Smart Mater. Struct.* **18** 095029

[16] Okayasu M, Aoki S and Mizuno M 2008 Effects of silver-based metal electroplate on fatigue properties of PZT ceramics *Int. J. Fatigue* **30** 1115–24

[17] Allag H and Yonnet J P 2008 3D Analytical calculation of the interactions between permanent magnets *Conf. Int. REPM (Rare Earth Permanent Magnets and their Applications) (Knossos, Greece)*

[18] Challa V R, Prasad M G and Fisher F T 2011 Towards an autonomous self-tuning vibration energy harvesting device for wireless sensor network applications *Smart Mater. Struct.* **20** 025004

[19] Nezhad-Ahmadi M R, Weale G, El-Agha A, Griesdorf D, Tumbush G, Hollinger A, Matthey M, Meiners H and Asgaran S 2008 A 2 mW 400 MHz RF transceiver SoC in 0.18 μm CMOS technology for wireless medical applications *IEEE Radio Frequency Integrated Circuits Symp., RFIC 2008 (Atlanta, GA)*

[20] Wong A C W, Kathiresan G, Chan C K T, Eljamaly O, Omeni O, McDonagh D, Burdett A J and Toumazou C 2008 A 1 V wireless transceiver for an ultra-low-power SoC for biotelemetry applications *IEEE J. Solid-State Circuits* **43** 1511–21